Hindawi
Geofluids
Volume 2022, Article ID 6167382, 11 pages
https://doi.org/10.1155/2022/6167382

Research Article

Thermodynamic Characteristics of CH_4 Adsorption on Shale at Different Temperatures

Pei Xue,[1,2] **Quansheng Liang**,[1] **Shiyan Hao**,[1] **Jintao Yin**,[1] **Chao Gao**,[1] **Lixia Zhang**,[1] **and Qianping Zhao**[1]

[1]*Research Institute, Shaanxi Yanchang Petroleum (Group) Co., Ltd., Xi'an, Shaanxi 710075, China*
[2]*Northwest University of Political Science and Law, Xi'an 710063, China*

Correspondence should be addressed to Pei Xue; gwl330@163.com

Received 15 May 2022; Revised 30 June 2022; Accepted 9 July 2022; Published 28 July 2022

Academic Editor: Dengke Liu

In order to clarify the effect of temperature on the isosteric heat of adsorption of CH_4 onto shale, by using the isothermal adsorption data of shale in the temperature range of 300~473 K and the pressure range of 0.08~14 MPa, the isosteric heat of adsorption is calculated, respectively, in the temperature range of 300~308 K, 338~373 K, and 423~473 K. The results show that the influence of temperature on the isosteric heat of adsorption of CH_4 onto shale is mainly reflected in three aspects: the variation range of the isosteric heat of adsorption, the absolute adsorption capacity at which the isosteric heat of adsorption reach the maximum, and the change rate of the isosteric heat of adsorption. Specifically, as the temperature range moves to a higher range, the variation range of the isosteric heat increases significantly, and the absolute adsorption capacity decreases. The curve shape of the change rate of the isosteric heat of adsorption in different temperature ranges remained the same (decreased first and then increased), but the change rate increased gradually as the temperature range moved to a higher temperature range.

1. Introduction

In recent years, the isosteric heat of adsorption of solid–gas adsorption system, as a key thermodynamic parameter for describing the industrial design such as mixed gas separation [1], gas storage [2], and adsorption refrigeration [3], has been widely used in the research field of the adsorption characteristics of unconventional natural gas (such as coalbed methane and shale gas) [4–16].

The existing studies [5–16] on the isosteric heat of adsorption in the field of unconventional natural gas use the isometric plotting method to calculate the isosteric heat of adsorption, which is based on the Clausius-Clapeyron equation. In this method, the function fitting (exponential or linear function) between the natural logarithm of pressure and the adsorption capacity ($\ln P - n_{ab}$) at different temperatures and between the natural logarithm of pressure and the reciprocal of temperature under different adsorption capacities is carried out successively through the adsorption isotherm of solid-gas adsorption system, and the isosteric heat of adsorption is calculated through the slope of $\ln P - 1/T$ curve [17]. The isosteric heat of adsorption obtained by this method reflects the variation characteristics of adsorption heat with the adsorption capacity under the temperature range which the adsorption isotherm obtained in and cannot reflect the influence of temperature on isosteric heat of adsorption. Since the adsorption isotherms of the same sample at different temperatures are obviously different [18], the isometric plotting method depends on the adsorption isotherm data, and the change of the adsorption isotherm data will directly affect the calculation results of the isosteric heat of adsorption [19], it can be inferred from the angle of the isosteric heat of adsorption calculation method that the temperature will affect the isosteric heat of adsorption. However, up to now, there has not been a quantitative analysis of the effect of temperature on the isosteric heat of adsorption.

To this end, the author used the isotherm adsorption data of the Bornholm shale to correct the excess adsorption

Table 1: Mineralogical characteristics of the experimental sample [17].

Quartz (%)	Plagioclase (%)	Potassium feldspar (%)	Limestone (%)	Siderite (%)	Pyrite (%)
44.4	1.0	1.3	0.5	0.4	1.4
Marcasite (%)	Mica (%)	Illite (%)	Illite/montmorillonite (%)	Kaolinite (%)	Chlorite (%)
0.8	9.5	5.9	29.9	0.7	4.2

capacity-pressure data into absolute adsorption capacity-fugacity data. Based on the data, the isosteric heats of adsorption of CH_4 in the temperature range of 300-308 K, 338-373 K, and 423-473 K were analyzed for the same shale by using the isometric plotting method. At the same time, the change rate of isosteric heat of adsorption is defined, the variation characteristics of isosteric heat of adsorption in different temperature ranges are analyzed, and the effect of temperature on the isosteric heat of adsorption of CH4 in shale is clarified.

2. Isothermal Adsorption Experiment

This paper is aimed at analyzing the effect of temperature on the isosteric heat of adsorption of CH_4 onto shale. Limited by the data requirements of the isometric plotting method for calculating the isosteric heat of adsorption, the adsorption isotherm of shale in a wide temperature range is needed. Therefore, the adsorption isotherm in the temperature range of 300–473 K proposed in reference [20] is adopted as the basic data for the calculation of the isosteric heat of adsorption.

2.1. Materials and Methods. The samples are from the shale of Well Skelbro-2 in Bornholm, Denmark (hereinafter referred to as Holm shale). The mineral composition of the experimental samples is mainly illite-montmorillonite and quartz and contains a large amount of mica (see Table 1). The particle density is 2.592 g/cm^3, the total organic carbon content is 6.35 ± 0.1%, the equivalent vitrinite reflectance is 2.26%, the specific surface area is 22.8 ± 1.6 m^2/g, and the total pore volume is 0.0176 ± 0.002 cm^3/g. The samples used in the experiment were broken samples with particle sizes of 0.5–1 mm. Before the experiment, the samples were dried for 24 h at 473.15 K [17].

The experimental temperature range was set to be 300-473 K, and a total of 11 temperature points were set to be 300 K, 303 K, 308 K, 318 K, 338 K, 358 K, 373 K, 389 K, 423 K, 448 K, and 473 K, respectively. The equilibrium pressure range was set to be 0.08 MPa–14 MPa. The isothermal adsorption amount under 17 equilibrium pressures was measured at different equilibrium temperatures. The isothermal adsorption experiment started from the maximum set temperature of 473 K and gradually reduced the experimental temperature to 300 K. The fluctuation range of equilibrium temperature was controlled at ±0.1 K. The Hiden Isochema Intelligent Manometric Instrument (IMI) of Hiden Isochema Ltd. was selected as the experimental equipment. The maximum test temperature of the instrument was 1046.15 K, and the maximum test pressure was 20 MPa. The adsorbed gas used in the experiment was CH_4 with purity of 99.995% [17]. Detailed sample characteristic parameters and experimental procedures can be found in reference [20].

2.2. Experimental Results. Figure 1 shows the isotherm adsorption curve of Holm shale. The adsorption capacity obtained from the isothermal adsorption experiment is the excess adsorption capacity [21, 22]. Therefore, the excess adsorption amount is represented by n_{ex} in Figure 2.

Since the critical temperature and critical pressure of CH_4 are 190.55 K and 0.59 MPa, respectively, the temperature range of the adsorption isotherm curve of Holm shale is 300-473 K, which belongs to the supercritical adsorption category. The state changes from gas phase to supercritical fluid, and at the same time, the excess adsorption curve in the higher pressure range shows a maximum point.

3. Correction of Absolute Adsorption Capacity-Fugacity Curve

The adsorption amount directly obtained by the isothermal adsorption experiment is the excess adsorption amount. The excess adsorption amount represents the adsorption amount of the actual adsorption phase density minus the gas phase density, and the absolute adsorption amount represents the actual adsorption amount of the solid-gas adsorption system. Since the excess adsorption capacity cannot reflect the real adsorption capacity of the adsorption system, its value is smaller than the absolute adsorption capacity that characterizes the real adsorption capacity [21]. Using the excess adsorption capacity as the basic data, the calculated isosteric heat of adsorption is higher [19]. And in the range of low gas pressure, i. e., low adsorption amount, the isosteric heat of adsorption is less than zero, which is obviously contrary to the physical phenomenon that the adsorption process is exothermic. Therefore, from the perspective of the rationality of the calculation results, the absolute adsorption capacity should be used as the basic data for the calculation of the isosteric heat of adsorption [19, 23].

At the same time, in the low pressure stage, the difference between pressure and fugacity is small, and pressure can be used to replace fugacity for thermodynamic characteristic analysis. However, with the increase of pressure, the difference between them increases. If the pressure is used as the basic data of equivalent adsorption heat calculation, the influence of gas intermolecular force in the calculation results will be too large [23]. Therefore, the absolute adsorption capacity-fugacity data is selected as the basic data for the calculation of isosteric heat of adsorption, and the excess adsorption capacity-pressure data expressed in Figure 2 is converted to the absolute adsorption capacity-fugacity data.

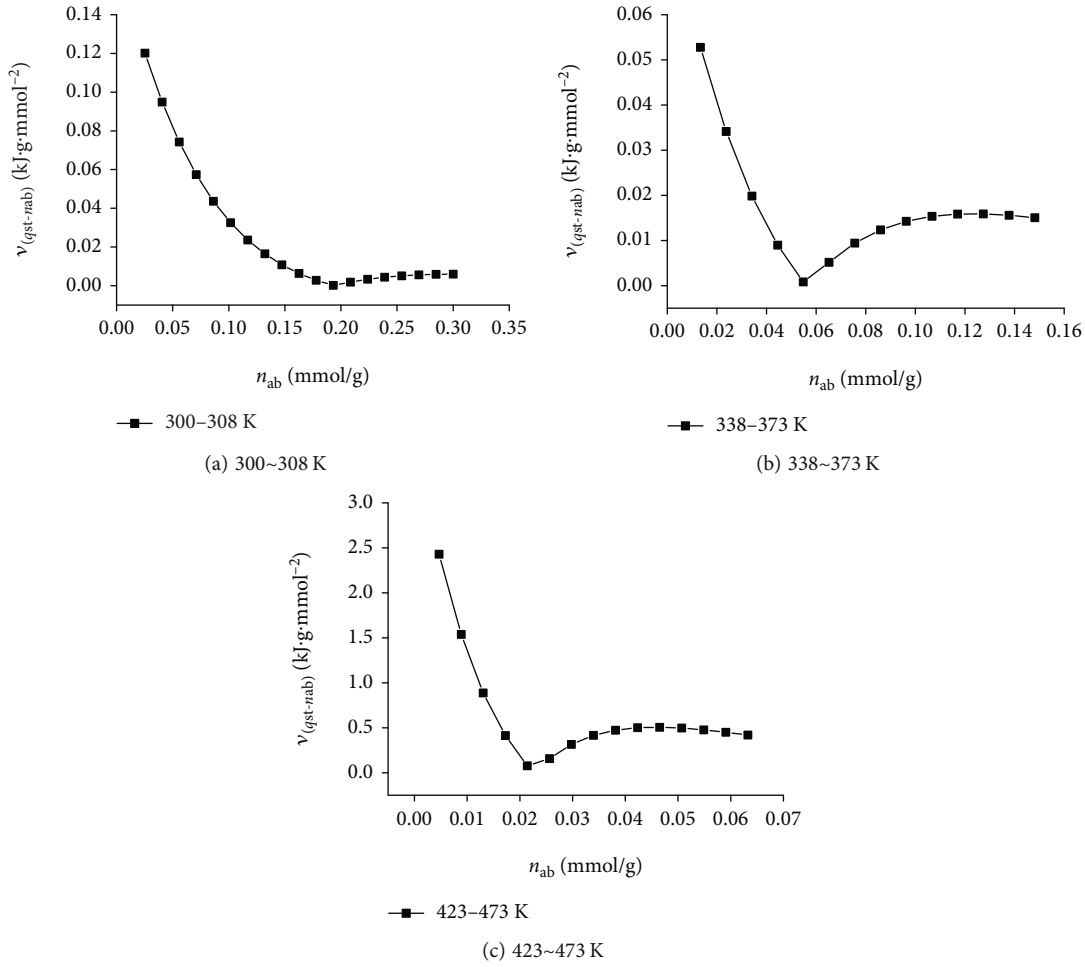

Figure 1: The change rate of isosteric heat of adsorption in different temperature range.

3.1. Correction of Absolute Adsorption Capacity. According to the definition of Gibbs adsorption capacity, the relationship between excess adsorption capacity and absolute adsorption capacity is [21, 23]

$$n_{ab} = \frac{n_{ex}}{1 - \left(\rho_g/\rho_a\right)}, \quad (1)$$

where n_{ab} is the absolute adsorption capacity (mmol/g). n_{ex} is the excess adsorption capacity (mmol/g). ρ_a is adsorption phase density (g/cm^3). ρ_g is gas phase density (g/cm^3). After determining the density of the gas phase and adsorption phase, Equation (1) can be used to correct the excess adsorption amount, so as to obtain the absolute adsorption curve. The vapor density of CH_4 used in this paper comes from the NIST database, as shown in Figure 3.

It can be seen from Figure 3 that at the same temperature, the gas density of CH_4 gradually increases with the increase of pressure. For example, at 300 K, when the pressure increases from 0.08 MPa to 13.08 MPa, the gas density of CH_4 increases from 0.00051523 g/cm^3 to 0.10123 g/cm^3. And in the same pressure, the gas density of CH_4 gradually decreases with the increase of temperature. For example, when the pressure is 5.46 MPa and the temperature rises from 300 K to 473 K, the gas density of CH_4 decreases from 0.03672 g/cm^3 to 0.02339 g/cm^3.

The adsorption phase density cannot be directly measured under supercritical conditions, and theoretical estimation and equation fitting calculation are mostly used. Reference [17] compared the accuracy of the existing adsorption phase density calculation methods, and the results showed that the calculation results of the empirical formula method were more reasonable. Therefore, the Ozawa empirical formula [24] was used to calculate the adsorption phase density, which can be expressed as

$$\rho_a = \rho_b \exp\left[-0.0025 \times (T - T_b)\right], \quad (2)$$

where ρ_b is the density at boiling point (g/cm^3), ρ_{b,CH_4} = 0.424g/cm^3. T_b is boiling temperature (K), T_{b,CH_4} = 111.65 K. T is absolute temperature (K). The calculated adsorption phase density curve of CH_4 is shown in Figure 4. In the temperature range of 300–473 K, the adsorption phase density of

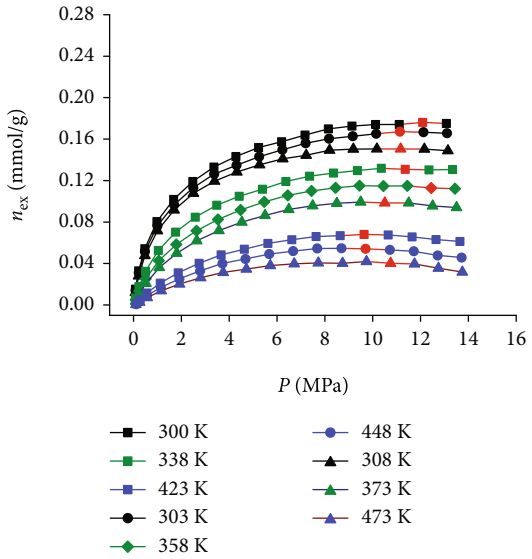

Figure 2: The adsorption isothermal of CH_4 onto shale (data cited from literature [20]).

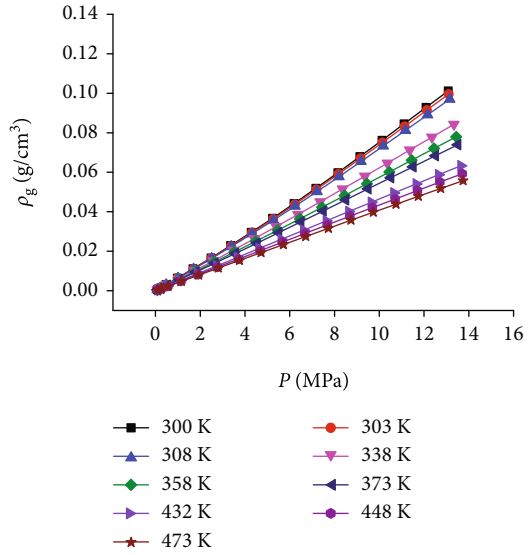

Figure 3: Gas phase density of CH_4.

CH_4 gradually decreased with the increase of temperature, from 0.26467 g/cm^3 at 300 K to 0.17174 g/cm^3 at 473 K.

The corrected absolute adsorption capacity curve is shown in Figure 5. It can be seen from Figure 5 that only when the temperature is 423 K, 448 K, and 473 K, the absolute adsorption amount curve has a maximum value. Theoretically, the absolute adsorption capacity curve represents the actual adsorption capacity. After the adsorption saturation is reached, the absolute adsorption capacity curve should remain stable, which is related to the adsorption phase density in the calibration process.

3.2. Calculation of Fugacity. Fugacity f and fugacity coefficient φ are important basic concepts in thermodynamic calculation of variable composition systems and important

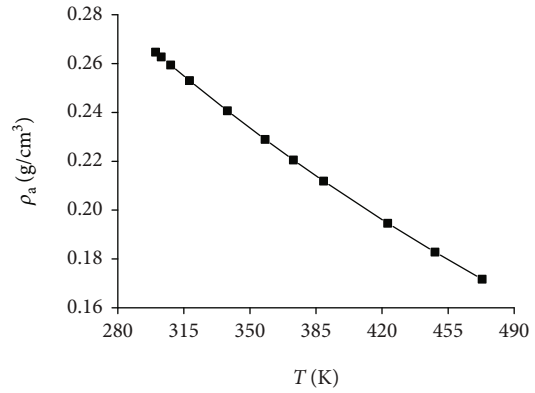

Figure 4: Adsorption phase density of CH_4.

tools for studying phase equilibrium and chemical reaction equilibrium [23, 25]. The relationship between fugacity and fugacity coefficient can be expressed as

$$T_{c,CH_4} = 190.55\ \text{K}, \tag{3}$$

where φ is fugacity coefficient. f is fugacity (Pa). p is pressure (Pa). In this paper, Peng-Robinson equation [26] of state is used to obtain fugacity; the fugacity coefficient [27] can be expressed as

$$\ln\varphi = Z - 1 + \ln\frac{RT}{ZRT - pb} - \frac{\sqrt{2}a(T)\alpha(T)}{4bRT}\ln\frac{ZRT + \left(\sqrt{2}+1\right)pb}{ZRT - \left(\sqrt{2}-1\right)pb}, \tag{4}$$

where $a(T)$ 为 is an intercohesion parameter and b is c -volume item. The intercohesion parameters can be expressed as

$$a(T) = \left(\frac{0.452724R^2T_c^{\ 2}}{p_c}\right)\cdot\alpha(T), \tag{5}$$

where T_c is critical temperature (K), $T_{c,CH_4} = 190.55$ K. P_c is critical pressure (Pa), $P_{c,CH_4} = 4.59$ MPa. $a(T)$ can be expressed as

$$\alpha(T) = \left[1 + k\left(1 - T_r^{\ 0.5}\right)\right]^2, \tag{6}$$

where T_r is the reduced temperature, $T_r = T/T_c$. When the eccentricity factor is $0 < \omega < 0.5$, k can be expressed as [23]

$$k = 0.3746 + 1.54226\omega - 0.26992\omega^2, \tag{7}$$

where ω is an eccentric factor, $\omega_{CH4} = 0.008$. b can be expressed as

$$b = \frac{0.07780RT_c}{p_c}. \tag{8}$$

The fugacity curve of CH_4 is shown in Figure 6 under the

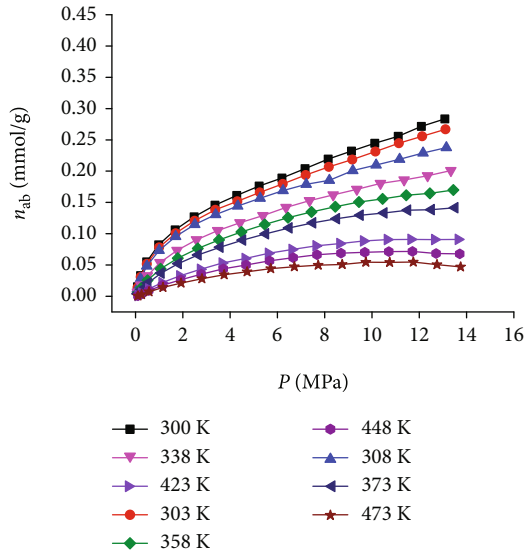

Figure 5: The absolute adsorption capacity curve.

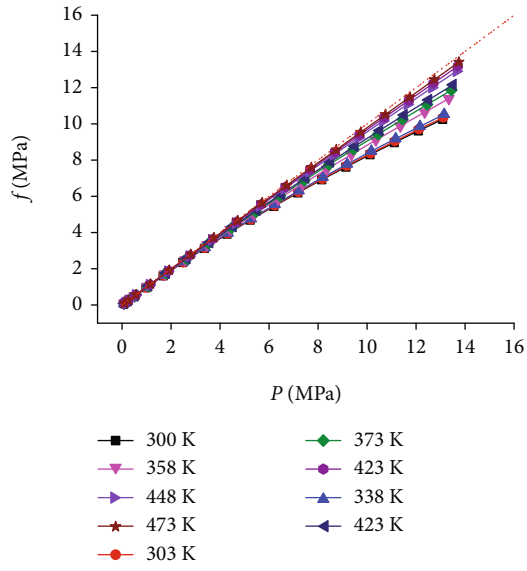

Figure 6: Fugacity curve of CH_4 (the red virtual line is characterized as $f = p$).

conditions of temperature range 300-473 K and pressure range 0.08-13.75 MPa. It can be seen from Figure 6 that with the increase of pressure, the fugacity gradually increases.

In the lower pressure range, the fugacity is equivalent to the pressure, and the fugacity curve is close to the $f = p$ line (the red dotted line in Figure 6). As the pressure increases, the fugacity is gradually smaller than the pressure, and the difference between the two increases [23].

3.3. Absolute Adsorption Capacity-Fugacity Curve. Using the correction method of absolute adsorption capacity and fugacity proposed in the above section, the excess adsorption capacity of Holm shale (see Figure 2) is corrected, respectively, and the absolute adsorption capacity-fugacity curve is obtained, as shown in Figure 7. The absolute adsorption curve has maximum value only at 448 K and 473 K.

4. Characteristics of the Isosteric Heat of Adsorption in Shale

The isosteric heat of adsorption is defined as the heat released by the adsorption of infinitely small gas molecules when the adsorption capacity is constant [17, 28]. Using the Clausius-Clapeyron equation, under the adsorption capacity (n), the isosteric heat of adsorption q_{st} can be expressed as [11, 17, 29, 30]

$$-\left(\frac{d\ln p}{dT}\right)_n = \frac{q_{st}}{RT^2}, \tag{9}$$

where p is the equilibrium adsorption pressure (Pa). Since the absolute adsorption capacity n_{ab} reflects the actual adsorption amount of the adsorption system, n_{ab} is used in the calculation of the equivalent adsorption heat [17, 30].

And the experimental pressure range obviously exceeds the pressure range suitable for the ideal gas assumption, and fugacity is used to replace the pressure in the thermodynamic analysis. Therefore, formula (9) can be rewritten as

$$-\left(\frac{d\ln f}{dT}\right)_{n_{ab}} = \frac{q_{st}}{RT^2}. \tag{10}$$

4.1. Calculation of Isosteric Heat of Adsorption Based on Adsorption Isosteric Plotting Method. The theoretical method of the adsorption isometric line plotting method is to integrate formula (10) when the adsorption amount is a fixed value and obtain

$$\ln f = -\frac{q_{st}}{RT} + M, \tag{11}$$

where M is a constant part of indefinite integral. It can be seen from equation (11) that $1/T$ and $\ln f$ have linear function characteristics, and the isosteric heat of adsorption q_{st} can be obtained by using the linear slope of the function ($-(q_{st}/R)$). Representing the slope of the linear function ($-(q_{st}/R)$ as A, that is, $-(q_{st}/R)$, the isosteric heat of adsorption is

$$q_{st} = -RA. \tag{12}$$

In the calculation process, the relationship between $\ln f$ and n_{ab} should be drawn first, and then, the fitting function should be determined according to the shape of the $\ln f - n_{ab}$ curve to fit the curve [17]. The fitting function of $\ln f - n_{ab}$ was used to calculate and draw the $\ln f - 1/T$ curve under different adsorption capacity, and the isosteric heat of adsorption in the corresponding temperature range was calculated by using the slope of the $\ln f - 1/T$ curve. From the data shown in Figure 6, the curve of $\ln f - n_{ab}$ of the Holm shale in the temperature ranges of 300-308 K, 338-373 K, and 423-473 K can be obtained, as shown in Figure 8.

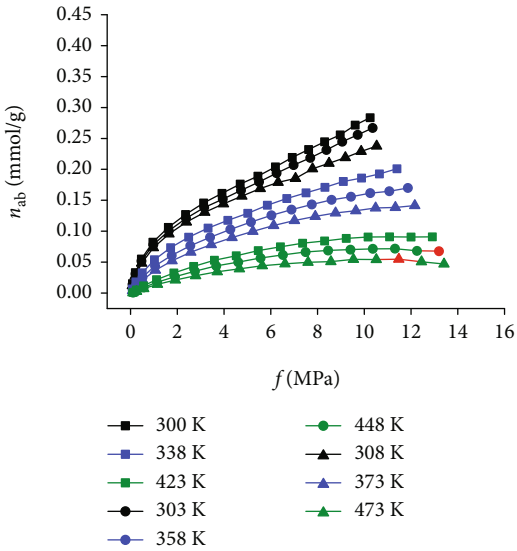

Figure 7: The curve of the absolute amount and fugacity.

According to the morphological characteristics of the $\ln f - n_{ab}$ curve, the exponential function was used to fit the $\ln f - n_{ab}$ curve (see Figure 8). The exponential function expression is

$$\ln f = a - bc^{n_{ab}}, \tag{13}$$

where a, b, and c are equation fit constant. The fitting results of the $\ln f - n_{ab}$ curve function (see Table 2) show that the data of $\ln f - n_{ab}$ maintained a good exponential function relationship at each temperature, and the correlation coefficient R^2 was greater than 0.98.

Although the exponential function can fit the $\ln f - n_{ab}$ curve well, the fitting correlation coefficient shows a decreasing trend with the increase of temperature, that is, from 0.99902 at 300 K to 0.98437 at 473 K.

From the shape of the $\ln f - n_{ab}$ curve (Figure 8), the reason is that at higher temperature (373–473 K), the data of $\ln f - n_{ab}$ gradually deviates from the fitting curve of the exponential function at the high adsorption of the curve (shown in Figure 7 by the red solid coil); that is, the positive increment of the ordinate of the data point does not meet the law of $d \ln f / dn_{ab} = -b \cdot \ln c \cdot c^{n_{ab}}$.

When the adsorption system has reached or is close to the saturated adsorption state, with the increase of fugacity f, the absolute adsorption capacity n_{ab} has tended to be stable, and the fitting accuracy of $\ln f - n_{ab}$ will decrease. From this point of view, when using the adsorption isotherm plotting method to calculate the isosteric heat of adsorption, the data in the adsorption isotherm indicating that the adsorption system has reached or approached the saturated adsorption state should be excluded.

In the temperature range of 300~308 K, 338~373 K, and 423~473 K, the value range of n_{ab} was set to be 0.01~0.3 mmol/g, 0.003~0.2 mmol/g, and 0.0005~0.08 mmol/g, and at the same time, twenty value points were set at equal intervals in the range of n_{ab} with different adsorption amounts, and then, the $\ln f - 1/T$ curves under different absolute adsorption amounts were drawn, as shown in Figure 9.

4.2. Isosteric Heat of Adsorption at Different Temperatures. A linear function is used to fit the $\ln f - 1/T$ curve under different temperature ranges and absolute adsorption capacity, and the linear fitting equation can be expressed as

$$\ln f = h + An_{ab}. \tag{14}$$

Figure 10 shows the linear fitting correlation coefficient curve of the $\ln f - 1/T$ curve in different temperature ranges that are significantly different. Specifically, in the range of 300-308 K, the fitting correlation coefficient R^2 is generally above 0.92, and the fitting effect is good. In the interval of 338~373 K and 423~473 K, the fitting correlation coefficient R^2 showed in the low adsorption stage ($n_{ab} < 0.1585$ mmol/g at 338~373 K and $n_{ab} < 0.0633$ mmol/g at 423~473 K). In the high value range in the interval of 0.8~0.99 and in the stage of high adsorption capacity ($n_{ab} \geq 0.1585$ mmol/g at 338~373 K, $n_{ab} \geq 0.0633$ mmol/g at 423~473 K), the correlation coefficient R^2 decreased rapidly with the increase of adsorption capacity and even negatively appeared at the position close to the maximum absolute adsorption capacity value (shown in red data in Figure 7). If the correlation coefficient $R^2 = 0.8$ is used as the criterion for judging whether the $\ln f - 1/T$ curve conforms to the linear law, the slope A of the linear fitting function of the $\ln f - 1/T$ curve in the range of $n_{ab} \geq 0.1585$ mmol/g at 338~373 K and $n_{ab} \geq 0.0674$ mmol/g at 423~473 K can no longer be used for the calculation of isosteric heat of adsorption.

In view of the above rules of the linear fitting correlation coefficient of the $\ln f - 1/T$ curve, in the subsequent calculation of the isosteric heat of adsorption using the linear fitting slope A value, this paper adopted the slope A value of the linear fitting of the $\ln f - 1/T$ curve in a temperature range of 300~308 K, 338~373 K, and 423~473 K, corresponding the range of n_{ab} is 0.01~0.3 mmol/g, 0.003~0.1482 mmol/g, and 0.0047~0.0591 mmol/g, to calculate isosteric heat of adsorption. The calculation results are shown in Figure 11.

It can be seen from Figure 11 that in different temperature ranges, with the increase of absolute adsorption amount, the isosteric heat of adsorption in each temperature range show a nonmonotonic change that first increases and then decreases. Specifically, in the lower temperature range of 300–308 K, q_{st} increased from 17.18642 kJ/mol at $n_{ab} = 0.01$ mmol/g to 24.55957 kJ/mol at $n_{ab} = 0.19316$ mmol/g and then decreased to $n_{ab} = 0.3$ 24.0695 kJ/mol at $n_{ab} = 0.3$ mmol/g. In the temperature range of 338~373 K, q_{st} increased from 9.43947 kJ/mol at $n_{ab} = 0.003$ mmol/g to 21.51892 kJ/mol at $n_{ab} = 0.05484$ mmol/g and then decreased to 9.19229 kJ/mol at $n_{ab} = 0.14816$ mmol/g. In the temperature range of 423~473 K, q_{st} increased rapidly from 3.21306 kJ/mol at $n_{ab} = 0.0005$ mmol/g to 25.56946 kJ/mol at $n_{ab} = 0.02142$ mmol/g and then decreased to 7.95283 kJ/mol at $n_{ab} = 0.06326$ mmol/g.

As the temperature range moves to a higher range, the variation range of the isosteric heat of adsorption increases significantly. For example, in the temperature range of

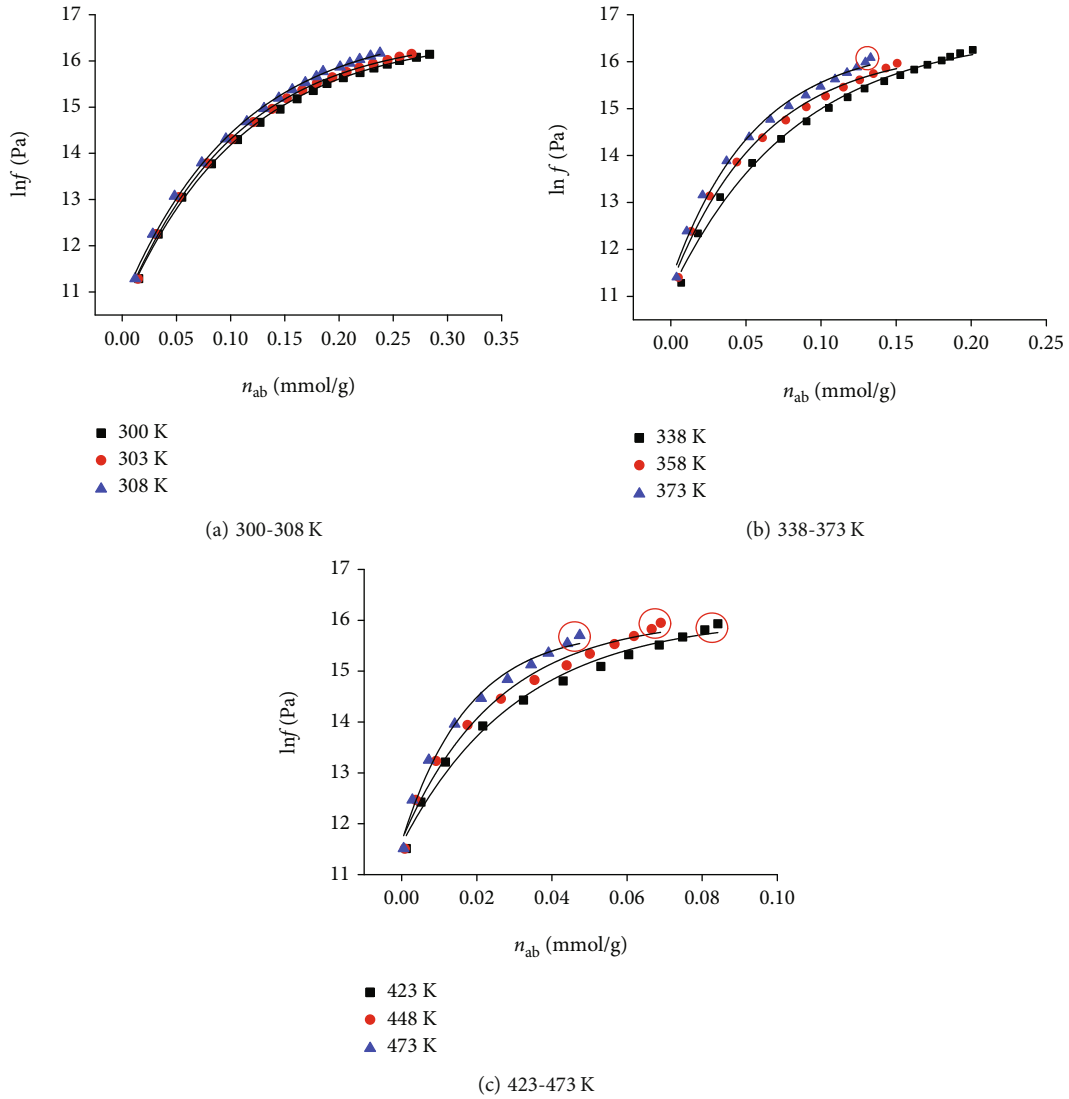

Figure 8: The curve of the exponential function fitting of $\ln f - n_{ab}$.

Table 2: The result of exponential function fitting of $\ln f - n_{ab}$.

Temperature (K)	Equation fitting parameters and correlation coefficients			
	a	b	c	R^2
300	16.55557	5.94858	1.02×10^{-4}	0.99902
303	16.57491	5.95977	6.39×10^{-5}	0.999
308	16.78271	6.01981	8.24×10^{-5}	0.99836
338	16.62614	5.53672	4.96×10^{-6}	0.99409
358	16.28054	5.0472	7.84×10^{-8}	0.99281
373	16.38241	5.04476	1.40×10^{-8}	0.99015
423	16.05466	4.45653	1.00×10^{-14}	0.98705
448	16.04904	4.37296	6.76×10^{-18}	0.98393
473	15.82416	4.17704	1.84×10^{-25}	0.98437

300~308 K, 338~373 K, and 423~473 K, the variation range of isosteric heat of adsorption is 17.18642~24.55957 kJ/mol, 2.60997~21.51892 kJ/mol, and 2.26209~25.56946 kJ/mol, respectively. The change amplitudes are 7.37315 kJ/mol, 18.90895 kJ/mol, and 23.30737 kJ/mol in turn.

And, as the temperature range moves to higher range, the absolute adsorption capacity ($n_{ab,q_{st-max}}$) when the maximum of the isosteric heat of adsorption appears gradually decreases. For example, the temperature range at 300~308 K, $n_{ab,q_{st-max}} = 0.19316$ mmol/g, and at the temperature range of 338~373 K and 423-473 K, $n_{ab,q_{st-max}}$ are 0.05484 mmol/g and 0.02142 mmol/g, respectively.

In order to quantitatively reflect the change rate of the isosteric heat of adsorption q_{st} with the absolute adsorption amount n_{ab} in different temperature ranges, the change rate of the isosteric heat of adsorption $v_{qst-nab}$ is defined, and its

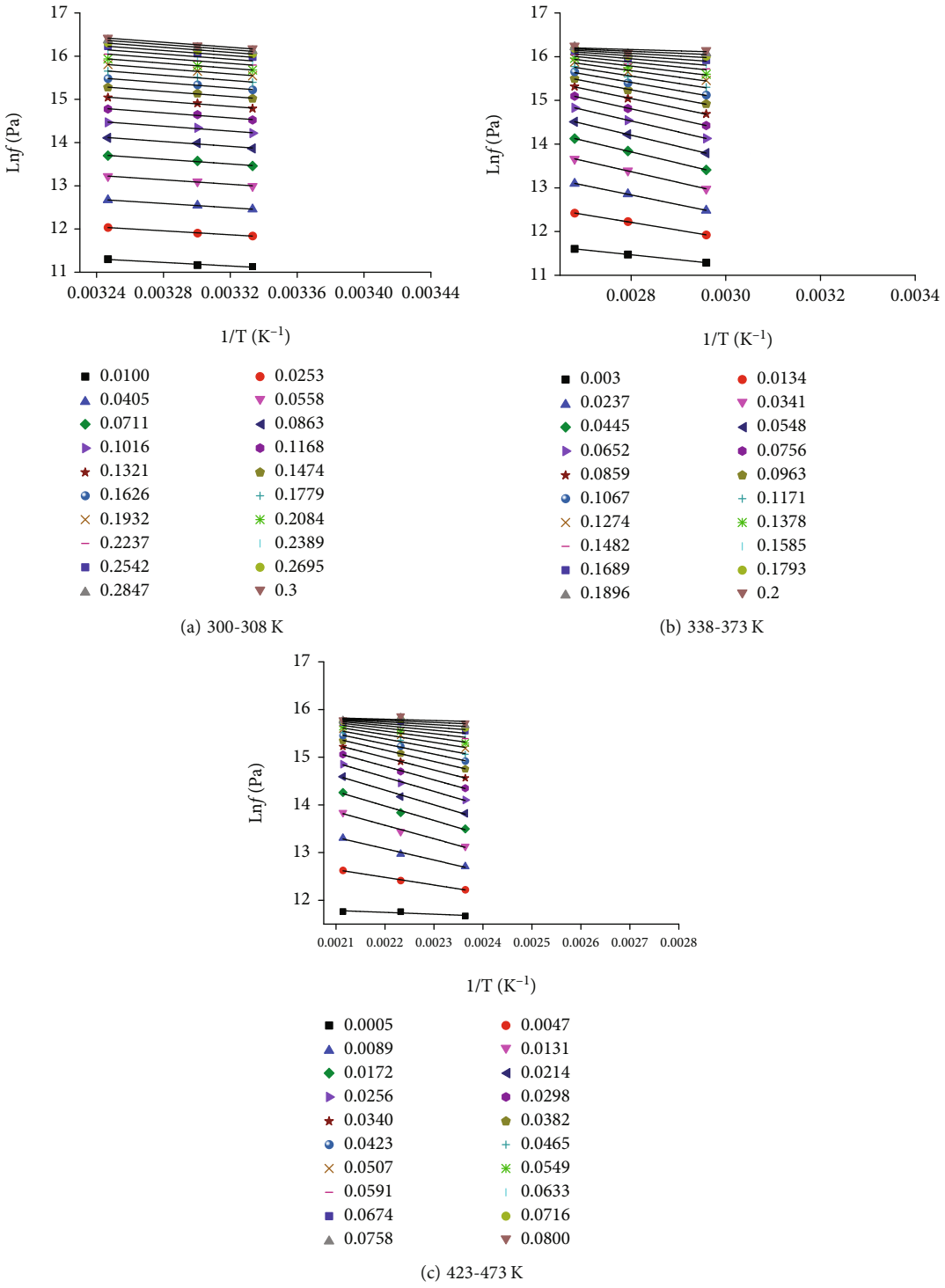

Figure 9: The cure of $\ln f - 1/T$ curve at different adsorption amounts.

expression is

$$v_{q_{st}-n_{ab}} = \left|\frac{\Delta q_{st}}{\Delta n_{ab}}\right| = \left|\frac{q_{sti+1} - q_{sti}}{n_{abi+1} - n_{abi}}\right|, \quad (15)$$

where $v_{q_{st}-n_{ab}}$ is the change rate of isosteric heat of adsorption (kJ·g·mmol^{-2}). According to the heat of isosteric curves in different temperature ranges (see Figure 10), combined with formula (15), the change rate of the isosteric heat of adsorption in different temperature ranges can be obtained (see Figure 1).

It can be seen from Figure 1 that the change rate of isosteric heat of adsorption in different temperature ranges shows a change law of first decreasing and then increasing and has a higher value in the stage of low adsorption

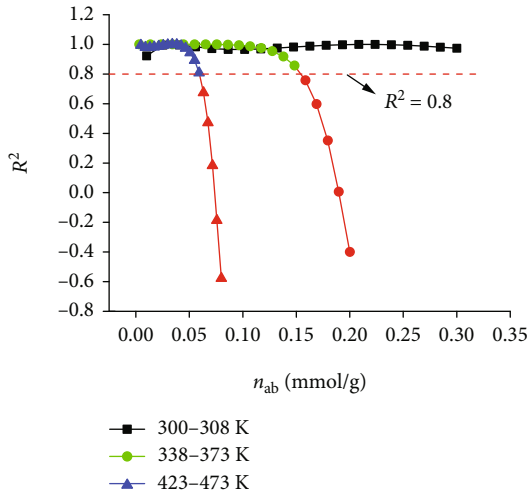

Figure 10: Correlation coefficient of $\ln f - 1/T$.

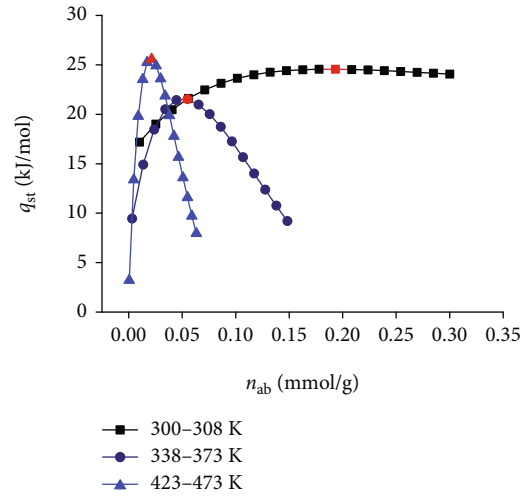

Figure 11: Isosteric heat of adsorption in different temperature ranges.

capacity. For example, in the temperature range of 330~308 K, the change rate ($v_{q_{st}-n_{ab}}$) decreases from 0.1201 kJ·g·mmol^{-2} when n_{ab} is 0.02526 mmol/g to 0.002 kJ·g·mmol^{-2}; when n_{ab} is 0.19316 mmol/g, then the rate of change increased to 0.0059 kJ·g·mmol^{-2} as n_{ab} increased to 0.3 mmol/g.

At the same time, the change rate of isosteric heat in the low temperature range is lower than that in the high temperature range. For example, when the temperature range is 300~308 K, 338~373 K, and 423~473 K, $v_{q_{st}-n_{ab}}$ is 0.0002~0.1201 kJ·g·mmol^{-2}, 0.0081~0.5277 kJ·g·mmol^{-2}, and 0.0765~2.4293 kJ·g·mmol^{-2}, respectively.

The variation trend of isosteric heat of adsorption is affected by the heterogeneity of adsorption sites and the interaction force between gas molecules [30–34]. When adsorbate molecules are adsorbed on a heterogeneous surface, they will preferentially adsorb to the strong adsorption sites with higher surface energy and then gradually adsorb to the adsorption sites with lower surface energy. This results in a decrease in the isosteric heat of adsorption curve with increasing adsorption capacity. At the same time, with the increase of the adsorption capacity, the intermolecular force of the adsorbate increases, causing the isosteric heat of adsorption to increase with the increase of the adsorption amount [17, 22, 23].

As shown in Figure 11, the isosteric heat of adsorption curve at different temperatures increases first and then decreases with the increase of absolute adsorption capacity. When the isosteric heat of adsorption curve reaches the maximum, the heterogeneity of the adsorbent surface and the effect of the intermolecular interaction of the adsorbate on the isosteric heat of adsorption reach a balance, and then, the heterogeneity of the adsorbent surface plays a dominant role, and the isosteric heat of adsorption decreases with the increase of the adsorption amount.

In addition, since the maximum of the isosteric heat of adsorption represents a balance between the heterogeneity of the shale surface and the effect of the intermolecular force of CH_4 on the isosteric heat of adsorption. Therefore, when the maximum of the isosteric heat of adsorption in the higher temperature range moves to the low adsorption capacity, it reflects the weakening of the intermolecular force of the adsorbate and the enhancement of the heterogeneity of the adsorbent surface with the increase of temperature.

5. Conclusion

The effect of temperature on the isosteric heat of adsorption of CH_4 in shale is mainly reflected in three aspects: the variation range, the maximum value, and the rate of change of the isosteric heat of adsorption. The following conclusions can be made:

(1) As the temperature range moves to a higher range, the variation range of the isosteric heat of adsorption increases significantly. For example, in the temperature range of 300~308 K, 338~373 K, and 423~473 K, the variation range is 7.37315 kJ/mol, 18.90895 kJ/mol, and 23.30737 kJ/mol, respectively

(2) As the temperature range moves to a higher range, the absolute adsorption capacity when the maximum of the isosteric heat of adsorption appears ($n_{ab,q_{st-max}}$) decreases gradually. For example, within the temperature range of 300~308 K, 338~373 K, and 423~473 K, $n_{ab,q_{st-max}}$ are 0.19316 mmol/g, 0.05484 mmol/g, and 0.02142 mmol/g, respectively

(3) The shape of the isosteric heat change rate remains the same in different temperature ranges (decreases first and then increases), but as the temperature range moves to a higher range, the isosteric heat of adsorption change rate gradually increases

Data Availability

The experimental data of adsorption isotherm are cited from ref. and marked in the text.

Conflicts of Interest

The authors declare that they have no conflicts of interest.

References

[1] D. G. Hartzog and S. Sircar, "Sensitivity of PSA process performance to input variables," *Adsorption-journal of the International Adsorption Society*, vol. 1, no. 2, pp. 133–151, 1995.

[2] C. Liu, Q. H. Yang, Y. Tong, H. T. Cong, and H. M. Cheng, "Volumetric hydrogen storage in single-walled carbon nanotubes," *Science*, vol. 80, no. 13, pp. 2389–2391, 2002.

[3] K. C. Ng, M. A. Sai, A. Chakraborty, B. B. Saha, and S. Koyama, "The electro-adsorption chiller: performance rating of a novel miniaturized cooling cycle for electronics cooling," *Transactions of the Asme Serie C Journal of Heat Transfer*, vol. 128, no. 9, pp. 889–896, 2006.

[4] A. Chakraborty, B. B. Saha, S. Koyama, and K. C. Ng, "On the thermodynamic modeling of the isosteric heat of adsorption and comparison with experiments," *Applied Physics Letters*, vol. 89, no. 17, p. 171901, 2006.

[5] Y. J. Cui, Q. L. Zhang, and X. L. Yang, "The change rules of adsorption capacity and isosteric heat of adsorption of different-coals," *Natural Gas Industry*, vol. 23, no. 7, pp. 130-131, 2007.

[6] Y. B. Lin, D. M. Ma, and Y. H. Liu, "Experiment of the influence of temperature on coalbed methane adsorption," *Coal Geology & Exploration*, vol. 6, pp. 24–28, 2012.

[7] S. Q. Lu, L. Wang, and L. M. Qin, "Analysis on adsorption capacity and adsorption thermodynamic characteristics of different metamorphic degree coals," *Coal Science and Technology*, vol. 6, pp. 130–135, 2014.

[8] G. W. Yue, Z. F. Wang, and B. Kang, "Prediciton for isothermal adsorption curve of coal/CH_4 based on adsorption heat theory," *Natural Gas Geoscience*, vol. 26, no. 1, pp. 148–153, 2015.

[9] G. Wei, W. Xiong, G. Shusheng, H. Zhiming, L. Honglin, and Y. Rongze, "Impact of temperature on the isothermal adsorption/desorption of shale gas," *Petroleum Exploration and Development*, vol. 40, no. 4, pp. 514–519, 2013.

[10] F. Yang, Z. F. Ning, Q. Wang, H. Liu, and D. Kong, "Thermodynamic analysis of methane adsorption on gas shale," *Journal of Central South University (Science and Technology)*, vol. 45, no. 8, pp. 2871–2877, 2014.

[11] Y. Feng, N. Zhengfu, L. Huiqing, and K. Detao, "Methane adsorption characteristics of gas shale," *Special Oil & Gas Reservoirs*, vol. 20, no. 5, pp. 133–136, 2013.

[12] L. I. Xiao-Yuan, C. A. O. Feng, Y. U. E. Gao-Fan, and L. I. Yang-Jie, "The experimental study of adsorption characterisitic of Carboniferous shale in Eastern Qaidam," *Earth Science Frontiers*, vol. 23, no. 5, pp. 95–102, 2016.

[13] C. A. O. Shi-liu, L. I. Ping, Z. H. A. N. G. Hui et al., "Comparison on adsorption and desorption thermodynamics features between shale gas and coalbed methane," *Coal Science and Technology*, vol. 43, no. 2, pp. 64–67, 2015.

[14] J. P. Bai, D. K. Zhang, and J. Q. Yang, "Thermodynamic characteristics of adsorption-desorption of methane in coal seam 3 at Sihe Coal Mine," *Journal of China Coal Society*, vol. 39, no. 9, pp. 1812–1819, 2014.

[15] S. Li, Y. Bai, H. Lin, M. Yan, and H. Long, "Molecular simulation of adsorption thermodynamics of multicomponent gas incoal," *Journal of China Coal Society*, vol. 43, no. 9, pp. 114–121, 2018.

[16] L. I. N. Haifei, W. E. I. Wenbin, L. I. Shugang, Y. A. N. Min, and B. A. I. Yang, "Experimental study on thermodynamics characteristics of CH_4 and CO_2 adsorption on coal," *China Safety Science Journal*, vol. 28, no. 6, pp. 129–134, 2018.

[17] X. Pei, Z. Lixia, L. Quansheng, S. Yi, C. Cheng, and T. Yanshuai, "Isothermal adsorption properties of supercritical methane on shale," *Narural Gas Geoscience*, vol. 31, no. 9, pp. 1261–1270, 2020.

[18] G. Wei, X. Wei, H. Gao Shusheng, L. H. Zhiming, and Y. Rongze, "Impact of temperature on the isothermal adsorption/desorption characteristics of shale gas," *Petroleum Exploration and Development*, vol. 40, no. 4, pp. 481–485, 2013.

[19] X. Pei, Q. Panwen, Y. Tianqi, S. Derui, Z. Lixia, and G. Dongcheng, "Adsorption thermodynamic property for CH_4 and CO_2 of shales based on absolute adsorption capacity," *Journal of Shandong University of Science and Technology (Natural Science)*, vol. 38, no. 5, pp. 21–30, 2019.

[20] T. F. Rexer, M. J. Benham, A. C. Aplin, and K. M. Thomas, "Methane adsorption on shale under simulated geological temperature and pressure conditions," *Energy & Fuels*, vol. 27, no. 6, pp. 3099–3109, 2013.

[21] Z. Shangwen, W. Hongyan, X. Huaqing, G. Wei, and L. Bin, "Difference between excess and absolute adsorption capacity of shale and a new shale gas reserve calculation method," *Natural Gas Industry*, vol. 36, no. 1, pp. 12–20, 2016.

[22] P. Xue, L. Zhang, Q. Liang, X. Sun, Q. Zhao, and P. Qi, "Thermodynamic characteristics of CH_4 adsorption by continental shale," *Natural Gas Industry*, vol. 39, no. 11, pp. 64–73, 2019.

[23] P. Xue, L. X. Zhang, Q. S. Liang et al., "Difference analysis of isosteric heat of methane adsorption on shale based on fugacity and pressure: a case study of Yanchang Formation in Yanchang exploration area," *Lithologic Reservoirs*, vol. 33, no. 2, pp. 171–179, 2021.

[24] S. Ozawa, S. Kusumi, and Y. Ogino, "Physical adsorption of gases at high pressure. IV. An improvement of the Dubinin–Astakhov adsorption equation," *Journal of Colloid and Interface Science*, vol. 56, no. 1, pp. 83–91, 1976.

[25] Z. Juecheng, "Discussion about fugacity definition of pure matter," *Journal of Shanghai University of Engineering Science*, vol. 18, no. 2, pp. 14–17, 2004.

[26] D. B. Robinson, D. Y. Peng, and Y. K. Chung, "The development of the Peng - Robinson equation and its application to phase equilibrium in a system containing methanol," *Fluid Phase Equilibria*, vol. 24, no. 1-2, pp. 25–41, 1985.

[27] Y. Zheng, Q. Li, C. Yuan et al., "Thermodynamic analysis of high-pressure methane adsorption on coal-based activated carbon," *Fuel*, vol. 230, pp. 172–184, 2018.

[28] A. L. Myers, "Thermodynamics of adsorption in porous materials," *AICHE Journal*, vol. 48, no. 1, pp. 145–160, 2002.

[29] Z. H. O. U. Yaping and Z. H. O. U. Li, "Experimental study on high pressure adsorption of hydrogen on activated carbon," *Science in China (Series B)*, vol. 36, no. 6, pp. 598–607, 1996.

[30] P. Xue, L. X. Zhang, Q. S. Liang, X. Sun, Q. Zhao, and P. Qi, "Thermodynamic characteristics of CH_4 adsorption by continental shale: a case study of the Upper Triassic Yanchang shale in the Yanchang-Gasfield, Ordos Basin," *Natural Gas Industry*, vol. 39, no. 11, pp. 64–73, 2019.

[31] D. M. Ruthven, *Principle of Adsorption and Adsorption Process*, John Wilev& Sons Inc, New York, 1984.

[32] D. Ren, L. Ma, D. Liu, J. Tao, X. Liu, and R. Zhang, "Control mechanism and parameter simulation of oil-water properties on spontaneous imbibition efficiency of tight sandstone reservoir," *Frontiers in Physics*, vol. 10, no. 10, article 829763, 2022.

[33] D. Ren, H. Zhang, Z. Wang, B. Ge, D. Liu, and R. Zhang, "Experimental study on microscale simulation of oil accumulation in sandstone reservoir," *Frontiers in Physics*, vol. 10, no. 10, article 841989, 2022.

[34] R. Wang, C. Yang, H. Ru, P. Wang, and Y. Yang, "Comparison of error in methane isotherm adsorption by volumetric method for shale and coal," *Unconventional Oil and Gas*, vol. 8, no. 3, pp. 43–48, 2021.